PROCEEDINGS OF SCIENCE

Recent KLOE results on radiative kaon decays

KLOE Collaboration*
presented by Matthew Moulson†
INFN Frascati, Italy
E-mail: moulson@lnf.infn.it

While measuring the ratio $R_K = \Gamma(K^{\pm}_{e2(\gamma)})/\Gamma(K^{\pm}_{\mu 2(\gamma)})$, the KLOE Collaboration has studied the radiative process $K_{e2\gamma}$. The ratio of the width for the $K_{e2\gamma}$ decay with a positively polarized photon from structure-dependent radiation to the inclusive $K_{\mu 2(\gamma)}$ width is found to be $1.484(68) \times 10^{-5}$. The observed radiation spectrum agrees with predictions from chiral perturbation theory and is in contrast with predictions based on the light front quark model. This result reduces the contribution to systematic uncertainties on measurements of R_K. In a separate study, KLOE has measured the ratio of the radiative $K_{e3\gamma}$ decay width to the inclusive $K_{e3(\gamma)}$ width to be $924(28) \times 10^{-5}$. The distribution in energy and angle of the radiative photon has been analyzed in an attempt to isolate the signature from interference of the inner-bremsstrahlung and structure-dependent amplitudes.

2009 KAON International Conference KAON09,
June 09 - 12 2009
Tsukuba, Japan

*F. Ambrosino, A. Antonelli, M. Antonelli, F. Archilli, P. Beltrame, G. Bencivenni, C. Bini, C. Bloise, S. Bocchetta, F. Bossi, P. Branchini, G. Capon, D. Capriotti, T. Capussela, F. Ceradini, P. Ciambrone, E. De Lucia, A. De Santis, P. De Simone, G. De Zorzi, A. Denig, A. Di Domenico, C. Di Donato, B. Di Micco, M. Dreucci, G. Felici, S. Fiore, P. Franzini, C. Gatti, P. Gauzzi, S. Giovannella, E. Graziani, M. Jacewicz, V. Kulikov, G. Lanfranchi, J. Lee-Franzini, M. Martini, P. Massarotti, S. Meola, S. Miscetti, M. Moulson, S. Müller, F. Murtas, M. Napolitano, F. Nguyen, M. Palutan, A. Passeri, V. Patera, P. Santangelo, B. Sciascia, A. Sibidanov, T. Spadaro, M. Testa, L. Tortora, P. Valente, G. Venanzoni, and R. Versaci.

†Speaker.

PoS(KAON09)035

1. $K^{\pm} \to e^{\pm}\nu(\bar{\nu})\gamma$ ($K_{e2\gamma}$)

The K_{e2} decay is strongly helicity suppressed. Its rate is therefore a sensitive probe for minute contributions from physics beyond the Standard Model (SM). This is particularly true of the ratio $R_K = \Gamma(K_{e2(\gamma)})/\Gamma(K_{\mu 2(\gamma)})$, which can be calculated in the SM without uncertainties from strong-interaction dynamics. A recent calculation, which includes $\mathcal{O}(e^2p^4)$ corrections in chiral perturbation theory (ChPT), gives $R_K^{\rm SM} = 2.477(1) \times 10^{-5}$ [1]. Deviations of R_K of up to a few percent are possible in minimal supersymmetric extensions of the SM with non-vanishing e-τ scalar-lepton mixing [2].

Additional photons in the K_{e2} final state can be produced via internal bremsstrahlung (IB) or structure-dependent (direct) emission (SD); the spectrum of the latter is sensitive to the structure of the kaon. Interference between the IB and SD processes is negligible [3]. By definition, R_K is IB inclusive and SD exclusive. However, since events with IB photons cannot be distinguished from those with SD photons, to compare data with the SM prediction at the percent level or better, sufficiently precise knowledge of the SD component is required.

Because of the helicity suppression of the IB channel, the contribution from the SD channel to the total width is approximately equal to that from IB [3]. Previous measurements give the SD rate with a relative uncertainty of 15% [4]. The KLOE Collaboration has recently submitted for publication a measurement of R_K to within 1.3% [5, 6], obtaining $R_K = 2.493(31) \times 10^{-5}$. The study of the SD radiation in $K_{e2\gamma}$ decay presented here was conducted in order to reduce the contribution to the systematic error on the KLOE measurement of R_K from the uncertainty in the SD rate, from 0.5% to 0.2%. The NA62 Collaboration has recently announced a preliminary measurement of R_K with a 0.6% error [7]. The uncertainty in the SD rate is the second-largest contribution to the overall systematic uncertainty on this result, so that the present study may help to reduce the uncertainty on the NA62 value of R_K as well.

Decays with SD radiation can proceed through vector and axial transitions, with effective couplings V and A, respectively:

$$\frac{d^2\Gamma_{\rm SD}(K_{e2\gamma})}{dxdy} = \frac{G_F^2\,|V_{us}|^2\,\alpha_{\rm em}M_K^5}{64\pi^2} \times \left[(V+A)^2 f_{\rm SD+}(x,y) + (V-A)^2 f_{\rm SD-}(x,y)\right]. \qquad (1.1)$$

Here, $x = 2E_\gamma^*/M_K$ and $y = 2E_e^*/M_K$ are the normalized photon and electron energies in the kaon rest frame; both lie between 0 and 1. The form factors $f_{\rm SD+}$ and $f_{\rm SD-}$ describe the hadronic-structure-dependent effects in the contributions to the decay intensity from the channels with positive and negative photon polarization, respectively. In the SD+ channel, the photon is preferentially emitted in the direction opposite to that of the $e^{\pm}$, and the $e^{\pm}$ momentum spectrum is hard, peaking above the endpoint of the p_e^* spectrum in K_{e3} decays at 228 MeV. (p_e^* is the $e^{\pm}$ momentum in the decay rest frame.) In the SD$-$ channel, the photon is preferentially emitted in the direction parallel to that of the $e^{\pm}$, and the $e^{\pm}$ has a softer momentum spectrum. This is illustrated in the Dalitz plots for each of the two contributions in Fig. 1. Because the contribution from the SD$-$ channel is completely submersed in $K_{e3(\gamma)}$ background, the present measurement is exclusively focused on the SD+ contribution, and events with $p_e^* < 200$ MeV are eliminated to reduce background.

The starting sample of $K_{e2(\gamma)}$ events (inclusive with respect to the presence of additional photons in the final state) is the same as that used in the KLOE measurement of R_K [5, 6]. Single-prong

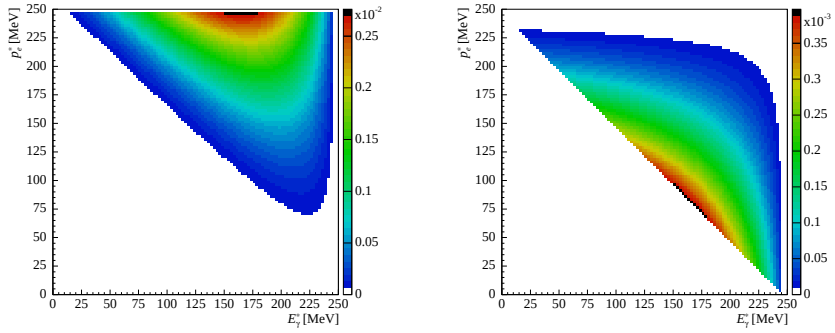

Figure 1: Plots of expected decay intensity in the (E_γ^*, p_e^*) plane corresponding to the contributions from the SD+ (left) and SD− (right) channels, evaluated from the $\mathcal{O}(p^4)$ ChPT calculation of Ref. [3].

vertices in the drift chamber are examined if the inbound track originates from the interaction point and has momentum compatible with the two-body decay momentum in $\phi \to K^+K^-$ (127 MeV), and if the outbound track has $p_{\rm lep} > 180$ MeV. The mass of the outbound track (the lepton candidate) is then reconstructed as $M^2_{\rm lep} = (E_K - |\mathbf{p}_{\rm miss}|)^2 - p^2_{\rm lep}$, with E_K the kaon energy and $\mathbf{p}_{\rm miss}$ the missing momentum at the vertex. Stringent track quality cuts on both the inbound and outbound tracks increase the ratio of $K_{e2(\gamma)}$ events to background events from 1/1000 to 1/20. For the analysis of R_K, the lepton-candidate track is extrapolated to the KLOE electromagnetic calorimeter, and a neural network is used to combine E/p, time-of-flight, and longitudinal energy deposition information for the purposes of μ/e separation.

For the analysis of $K_{e2\gamma}$, a hard cut is made on the neural-network output. The radiative photon must be explicitly detected as a cluster not associated to any track, with $E_\gamma^{\rm cal} > 20$ MeV as measured in the calorimeter. This reduces background from activity in accidental coincidence with the event and from cluster fragments. Furthermore, the times of arrival of the lepton and photon clusters must be consistent with each other (given the event topology) to within 2σ, or about 100 ps. This rejects $K \to \pi\pi^0$ events, in which the "lepton" is actually a pion, and travels with $\beta = 0.8$ instead of $\beta \approx 1$, so that its cluster arrives late. It also rejects $K_{\mu 2}$ events with accidental clusters, since the arrival times of such clusters are distributed evenly.

After the above cuts, the dominant backgrounds are from $K_{\mu 2(\gamma)}$ events for $M^2_{\rm lep} < 20000$ MeV^2, and from $K_{e3(\gamma)}$ events for $M^2_{\rm lep} > 20000$ MeV^2. $K_{e2\gamma}$ events with $p_e^* < 200$ MeV are submerged in background, as suggested by the left panel of Fig. 2. For the purposes of this analysis, the signal sample of SD+ events is fiducially defined as the sample of identified $K_{e2\gamma}$ events with $E_\gamma^* > 10$ MeV, $\cos\theta_\gamma^* < 0.9$ (θ_γ^* is the angle of the photon momentum with respect to that of the $e^\pm$), and $p_e^* > 200$ MeV. Simulations indicate that this selection has a 90% acceptance for true SD+ events, a 2% acceptance for SD− events, and contains a 1% background of IB events.

An additional variable that is useful in isolating signal events is ΔE_γ, the difference between the energy of the radiative photon as determined by kinematic closure using the tracks in the event, and that from the direct measurement of the energy with the calorimeter. On average, the photon energy is determined with a resolution of about 12 MeV in the former case and about 30 MeV in the latter. Since the $K_{e2\gamma}$ kinematics are built into this variable, it is particularly useful in separating $K_{e2\gamma}$ from $K_{e3(\gamma)}$ events, as seen in the right panel of Fig. 2.

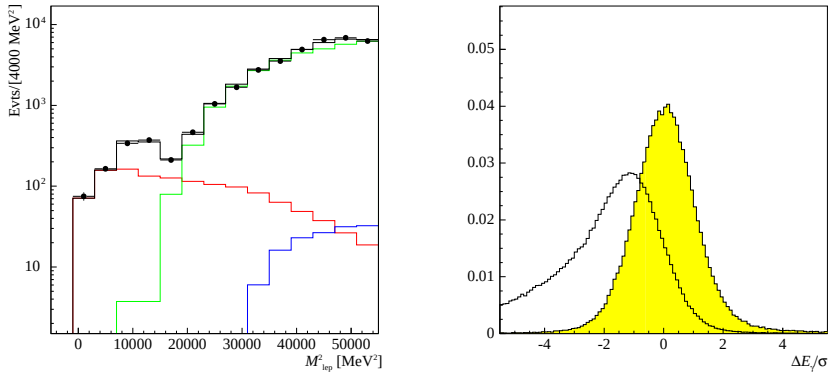

Figure 2: Left: Distributions of $M^2_{\rm lep}$ for $K_{e2\gamma}$ candidates and backgrounds. The distributions for simulated $K_{e2\gamma}$ events with $E^*_\gamma > 10$ MeV and $p^*_e > 200$ MeV ($p^*_e < 200$ MeV) are shown in red (blue). The expected contribution from $K_{e3(\gamma)}$ events is shown in green; that from all sources combined is shown in black. The peak at $M^2_{\rm lep} \approx 10000$ MeV$^2 \approx m^2_\mu$ is from $K_{\mu 2}$ events. The points with error bars are the data. Right: $\Delta E_\gamma/\sigma$ for simulated $K_{e2\gamma}$ events (yellow shaded histogram) and $K_{e3(\gamma)}$ events (open histogram).

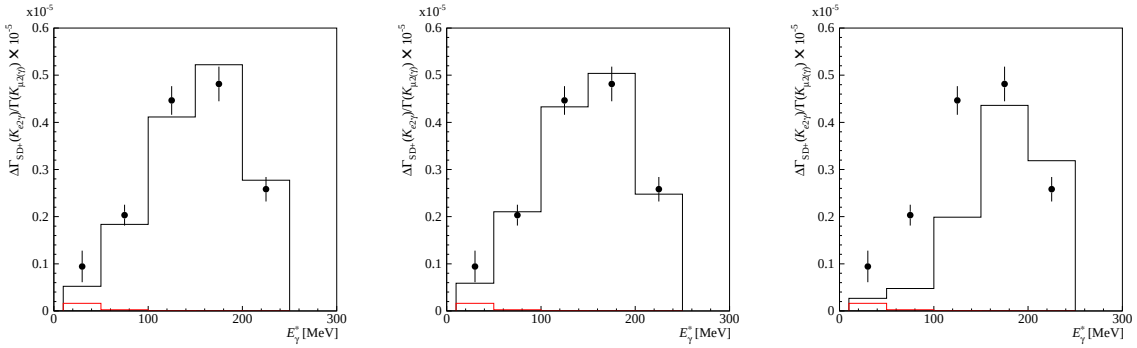

Figure 3: $\Delta\Gamma_{\rm SD+}(K_{e2\gamma})/\Gamma(K_{\mu 2(\gamma)})$ for five bins in E^*_γ, with model predictions. Left: Overlay (not a fit) of $\mathcal{O}(p^4)$ ChPT prediction. Middle: Fit with $\mathcal{O}(p^6)$ ChPT prediction to obtain normalization and slope of vector form factor. Right: Overlay (not a fit) of LFQM prediction with parameters as in Ref. [8]. Red histograms show expected contribution from IB.

The number of $K_{e2\gamma}$ events in the SD+ sample is determined via log-likelihood fits to the distribution of candidate events in the ($M^2_{\rm lep}$, ΔE_γ) plane in five different bins in E^*_γ. The first bin in E^*_γ extends from 10 to 50 MeV; the remaining four adjacent bins are 50 MeV wide. The fit function is a linear combination of Monte Carlo (MC) distributions for $K_{e2\gamma}$ events with kinematics as generated satisfying the SD+ selection (signal events), $K_{e2\gamma}$ events as generated not satisfying the SD+ selection (dominantly IB events), $K_{\mu 2(\gamma)}$ events (including those with background photons in accidental coincidence), and events from other background sources (mainly $K_{e3(\gamma)}$). All events in the input distributions satisfy the analysis cuts for the SD+ selection as reconstructed. The free parameters of the fit are the weights for each distribution.

Figure 3 summarizes the results of this analysis. The points in each panel show the measured values of $\Delta\Gamma_{\rm SD+}(K_{e2\gamma})$, normalized to $\Gamma(K_{\mu 2(\gamma)})$, for each of the five bins in E^*_γ. Summed over all bins in E^*_γ, $N_{\rm SD+}(K_{e2\gamma}) = 1378 \pm 63$, which gives $\Gamma_{\rm SD+}(K_{e2\gamma})/\Gamma(K_{\mu 2(\gamma)}) = 1.484(66)_{\rm st}(16)_{\rm sy} \times 10^{-5}$. This agrees with the prediction from the KLOE MC, 1.447×10^{-5}, which is based on

the $\mathscr{O}(p^4)$ ChPT calculation of Ref. [3], in which V and A in Eq. (1.1) are the constant values $0.095/m_K$ and $0.043/m_K$. In the left panel of the figure, the $\mathscr{O}(p^4)$ result is overlaid with the data; as an index of the agreement, $\chi^2/\text{ndf} = 5.4/5$. On the basis of this agreement, the KLOE MC is determined to be accurate in its description of the SD radiation in $K_{e2\gamma}$ decay to within the 4.6% relative uncertainty of the measurement. This reduces the corresponding contribution to the relative uncertainty on the value of R_K to 0.2% [5, 6].

At $\mathscr{O}(p^6)$, the vector coupling V in Eq. (1.1) depends linearly on the photon energy x, with $V = V_0[1+\lambda(1-x)]$, $V_0 = 0.082/m_K$ and $\lambda = 0.4$; the axial coupling is constant, $A \approx 0.034/m_K$ [8]. The middle panel of Fig. 3 shows the data together with the results of a fit using the $\mathscr{O}(p^6)$ prediction. Since there is no sensitivity to the SD$-$ component of the radiation, the quantity $(V-A)$ in Eq. (1.1) is fixed to its $\mathscr{O}(p^6)$ numerical value, and the fit parameters are (V_0+A) and λ. The results $(V_0+A) = 0.125(7)/m_K$ and $\lambda = 0.38 \pm 0.21$ with $\rho = -0.93$ and $\chi^2/\text{ndf} = 1.97/3$ are obtained. The right panel of Fig. 3 shows the data together with the results of a fit incorporating the light front quark model (LFQM) [8], which features a complicated dependence of V and A on x, with $V = A = 0$ at $x = 0$. The data are clearly in disagreement with the prediction of this model, as the overlay gives $\chi^2/\text{ndf} = 127/5$.

2. $K_L \to \pi^\mp e^\pm \nu(\bar{\nu})\gamma$ ($K_{e3\gamma}$)

The study of the $K_{e3\gamma}$ decay provides the opportunity to quantitatively test predictions from ChPT. In addition, precision measurements of the fully inclusive $K_{\ell 3(\gamma)}$ decay rates are needed for the determination of the CKM matrix element $|V_{us}|$. Such measurements require an accurate understanding of the radiation in these decays.

As in the case of $K_{e2\gamma}$ decays, the relevant kinematic variables for the study of $K_{e3\gamma}$ decays are E_γ^* and θ_γ^*. The IB amplitudes diverge for $E_\gamma^* \to 0$. The IB spectrum in θ_γ^* is peaked near zero as well, since $m_e \approx 0$. The IB and SD amplitudes interfere. The contribution to the width from IB-SD interference is 1% or less of the purely IB contribution; the purely SD contribution is negligible.

In the $\mathscr{O}(p^6)$ ChPT treatment of Ref. [9], SD radiation is characterized by eight amplitudes, $\{V_i, A_i\}$, which in the one-loop approximation are real functions. These terms have similar photon energy spectra, with maxima around $E_\gamma^* = 100$ MeV. This suggests the following decomposition of the photon spectrum:

$$\frac{d\Gamma}{dE_\gamma^*} = \frac{d\Gamma_{\text{IB}}}{dE_\gamma^*} + \sum_{i=1}^{4}\left(\langle V_i\rangle\frac{d\Gamma_{V_i}}{dE_\gamma^*} + \langle A_i\rangle\frac{d\Gamma_{A_i}}{dE_\gamma^*}\right) \simeq \frac{d\Gamma_{\text{IB}}}{dE_\gamma^*} + \langle X\rangle f(E_\gamma^*). \tag{2.1}$$

The function $f(E_\gamma^*)$ summarizes the effect of the SD amplitude; the parameter $\langle X\rangle$ measures its strength. The $\mathscr{O}(p^6)$ ChPT estimate is $\langle X\rangle = -1.2 \pm 0.4$. The low-energy constants (LECs) for the $\mathscr{O}(p^6)$ terms are unknown. An educated guess of their size leads to the assignment of an uncertainty on $\langle X\rangle$ of 30% of the $\mathscr{O}(p^4)$ result.

KLOE has studied the double differential rate in $K_{e3\gamma}$ decays, $d^2\Gamma/dE_\gamma^* d\theta_\gamma^*$, and measured the ratio R, conventionally defined as

$$R \equiv \frac{\Gamma(K_{e3\gamma}; E_\gamma^* > 30\text{ MeV}, \theta_\gamma^* > 20^\circ)}{\Gamma(K_{e3(\gamma)})}, \tag{2.2}$$

The value of this ratio has been computed at $\mathcal{O}(p^6)$ in ChPT, leading to the prediction [10]

$$R = (0.963 + 0.006\,\langle X\rangle \pm 0.010) \times 10^{-2}. \tag{2.3}$$

For $\langle X\rangle = -1.2$, $R = (0.96 \pm 0.01) \times 10^{-2}$, as quoted in Ref. [9]. The simultaneous measurement of R and $\langle X\rangle$ allows a precise comparison with the theory, in large part avoiding complications from the uncertainties on the LECs for $\mathcal{O}(p^6)$.

A first attempt to measure both R and the magnitude of the SD contribution was performed by the KTeV collaboration in 2001 [11]. They obtained $R = (0.908 \pm 0.008^{+0.013}_{-0.012}) \times 10^{-2}$; the analysis of the SD radiation was complicated by the use of a cumbersome theoretical framework. The KTeV data were subsequently reanalyzed using more restrictive cuts that provide better control over systematic effects, but which reduce the statistics by a factor of three. The more recent KTeV result is $R = (0.916 \pm 0.017) \times 10^{-2}$ [12]. No further attempt was made to isolate the SD component. In 2005, NA48 measured $R = (0.964 \pm 0.008^{+0.011}_{-0.009}) \times 10^{-2}$ [13], again without attempting to isolate the SD radiation.

The KLOE MC generates only radiation from IB, so the $\mathcal{O}(p^6)$ generator of Ref. [9] was used for the present analysis. The KLOE generator [14], makes use of a resummation in the soft-photon limit to all orders in α of the $\mathcal{O}(p^2)$ amplitude for single-photon emission. It is claimed to describe the IB photon spectrum at the level of $\sim$1%. While this is appropriate for inclusive decay-rate measurements at the 0.1% level, the SD contribution is about 1% of the IB contribution, so that the accuracy level of the KLOE IB generator is of about the same order as the SD contribution itself. Therefore, in this analysis, the generator of Ref. [9] is used to obtain the photon spectrum from IB as well as from SD.

The analysis is fully described in Ref. [15]. The criteria used to select an inclusive sample of $K_{e3\gamma}$ events are the same described in Ref. [16]. Vertices in the drift chamber along an expected line of flight reconstructed from a $K_S \to \pi^+\pi^-$ decay are identified as candidate K_L decays. Loose kinematic cuts are applied to remove background from $K_L \to \pi^+\pi^-\pi^0$ and $K_L \to \pi^+\pi^-$. A large amount of $K_{\mu 3(\gamma)}$ background is rejected using the variable $\Delta_{\pi\mu}$, the lesser value of $|E_{\rm miss} - p_{\rm miss}|$ calculated in the $\pi\mu$ and $\mu\pi$ track mass hypotheses. Events are retained only if $\Delta_{\pi\mu} > 10$ MeV. The difference between the times of flight of the hypothetical $e^\pm$ and $\pi^\mp$ tracks is used to purify the sample to about 99.3%.

Signal $K_{e3\gamma}$ events are selected from within the inclusive sample. Events are first required to contain a calorimeter cluster not associated with any track. The arrival time of this cluster must be within 8σ of the time expected on the basis of the position of the decay vertex and the photon time of flight. If there is more than one photon candidate, that with the most compatible timing is used. Once the photon has been identified, the requirement $\theta^*_\gamma > 20^\circ$ is enforced. The photon energy in the laboratory system is calculated from the track momenta and the photon cluster position, using the constraint that $m_\nu = 0$. The resolution obtained is $\sim$1 MeV, or about a factor of ten better than that of the energy measurement from the calorimeter. To check the agreement between MC and data on the reconstruction performance for quantities used for photon selection and to correct the MC efficiency, $K_L \to \pi^+\pi^-\pi^0$ events are used as a control sample.

Neural-network discriminators are used to reduce backgrounds from $K_L \to \pi^+\pi^-\pi^0$ and $K_{\mu 3(\gamma)}$. The neural network used to identify $K_L \to \pi^+\pi^-\pi^0$ events makes use of E^*_γ, θ^*_γ, the track momenta,

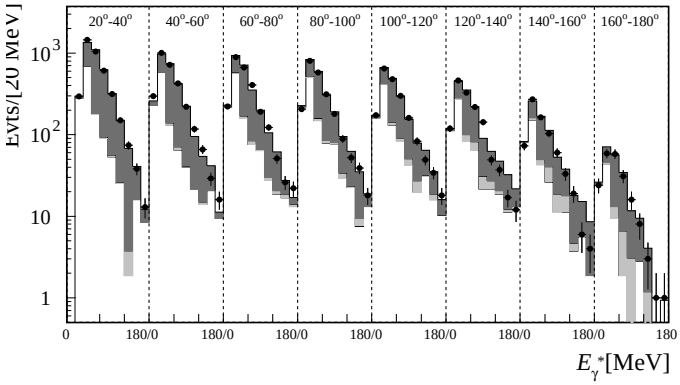

Figure 4: Results of fit to $(E_\gamma^*, \theta_\gamma^*)$ distribution: dots show data, dark gray region shows contribution from $K_{e3\gamma}$ events (IB and SD) satisfying kinematic cuts, white region shows contribution from $K_{e3\gamma}$ events not satisfying cuts, light gray region shows contribution from background.

the missing momentum, and $M_{\gamma\nu}^2$, the invariant mass of the photon-neutrino pair. The neural network used to identify $K_{\mu 3(\gamma)}$ events is based on the track momenta, the calorimeter energy measurement, and the depth of penetration into the calorimeter of the cluster centroid.

To count the numbers of $K_{e3\gamma}$ events from IB and SD, a fit to the experimental distribution in $(E_\gamma^*, \theta_\gamma^*)$ is performed using the sum of four independently normalized MC distributions: the distribution for $K_{e3\gamma}$ events from IB that satisfy the cuts on E_γ^* and θ_γ^* as generated; the distribution corresponding to the function $f(E_\gamma^*)$ in the second term of Eq. (2.1), representing the modification of the spectrum from SD events; $K_{e3\gamma}$ events from IB that satisfy the kinematic cuts only as reconstructed (and not as generated); and physical background from $K_L \to \pi^+\pi^-\pi^0$ and $K_{\mu 3(\gamma)}$ events. The free parameters of the fit are the number of IB events, the effective number of SD events (the integral of the spectral distortion induced by the IB-SD interference), and the number of $K_{e3\gamma}$ events not satisfying the kinematic cuts. The magnitude of the background contribution is fixed using the MC. Figure 4 shows the result of the fit. The two-dimensional distributions are plotted on a single axis; the E_γ^* distributions for each of the eight slices in θ_γ^* are arrayed sequentially. The fit gives $\chi^2/\text{ndf} = 60/69$ ($P = 77\%$), with $N_{\text{IB}}(K_{e3\gamma}) = 9083 \pm 213$, $N_{\text{SD}}(K_{e3\gamma}) = -102 \pm 59$, and an additional 6726 ± 194 $K_{e3\gamma}$ feed-down events not satisfying the kinematic cuts. The negative value for the effective number of SD events is a result of the destructive interference between the IB and SD amplitudes. The value $R = 924(23)_{\text{st}}(16)_{\text{sy}} \times 10^{-5}$ is obtained. The value of the parameter $\langle X \rangle$ defined in Eq. (2.1) is derived from the result of the fit, taking into account the small difference in the overall detection efficiencies for IB and SD events. The result is $\langle X \rangle = -2.3 \pm 1.3_{\text{st}} \pm 1.4_{\text{sy}}$. The 1σ contour is illustrated as the open ellipse in Fig. 5.

The dependence of R on $\langle X \rangle$ of Eq. (2.3) is shown in Fig. 5 as the diagonal shaded band. This dependence can be used to further constrain the possible values of R and $\langle X \rangle$ from this measurement, giving the 1σ contour illustrated as the filled ellipse in the figure. The constraint is applied via a fit, which gives $R = 944(14) \times 10^{-5}$ and $\langle X \rangle = -2.8 \pm 1.8$, with correlation $\rho = 72\%$ and $\chi^2/\text{ndf} = 0.64/1$ ($P = 42\%$). This result represents an improved test of ChPT with respect to that obtained using the measurements of R from Refs. [12, 13].

Finally, to test the accuracy of the KLOE IB generator [14], fits to the data with no SD com-

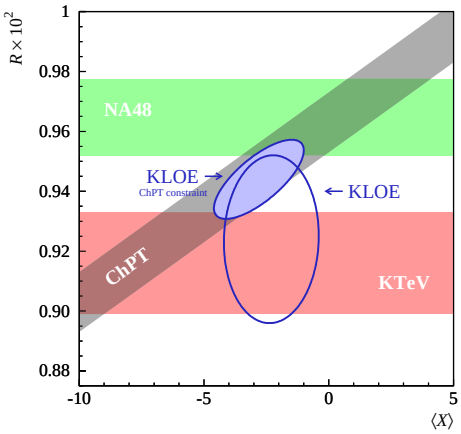

Figure 5: KLOE 1σ contours in the $(R, \langle X \rangle)$ plane from fit to the $(E_\gamma^*, \theta_\gamma^*)$ distribution (open ellipse), and same results when combined with constraint from ChPT (filled ellipse). Results from KTeV [12] and NA48 [13] are also shown, as well as the dependence of R on $\langle X \rangle$ used as the constraint.

ponent have been performed. The results $R = 921(23)_{\rm st} \times 10^{-5}$ for the KLOE generator [14] and $R = 925(23)_{\rm st} \times 10^{-5}$ for the $\mathcal{O}(p^6)$ generator of Ref. [9] have been obtained. This confirms the reliability of the KLOE generator for IB events.

References

[1] V. Cirigliano, I. Rosell, Phys. Rev. Lett 99 (2007) 231801.

[2] A. Masiero, P. Paradisi, R. Petronzio, Phys. Rev. D 74 (2006) 011701(R).

[3] J. Bijnens, et al., in: L. Maiani, G. Pancheri, N. Paver (Eds.), Second DA˘NE Physics Handbook, Laboratori Nazionali di Frascati, 1995, p. 315.

[4] J. Heintze, et al., Nucl. Phys. B 149 (1979) 365.

[5] KLOE Collaboration, F. Ambrosino, et al., arXiv:0907.3594 (2009).

[6] B. Sciascia for the KLOE Collaboration, these proceedings.

[7] E. Goudzovski for the NA62 Collaboration, these proceedings.

[8] C.-H. Chen, C.-Q. Geng, C.-C. Lih, Phys. Rev. D 77 (2008) 014004.

[9] J. Gasser, et al., Eur. Phys. J. C 40 (2005) 205–227.

[10] B. Kubis, private communication.

[11] KTeV Collaboration, A. Alavi-Harati, et al., Phys. Rev. D 64 (2001) 112004.

[12] KTeV Collaboration, T. Alexopoulos, et al., Phys. Rev. D 71 (2005) 012001.

[13] NA48 Collaboration, A. Lai, et al., Phys. Lett. B 605 (2005) 247–255.

[14] C. Gatti, Eur. Phys. J. C 45 (2006) 417.

[15] KLOE Collaboration, F. Ambrosino, et al., Eur. Phys. J. C 55 (2008) 539.

[16] KLOE Collaboration, F. Ambrosino, et al., Phys. Lett. B 636 (2006) 166–172.